x-ray transients containing accreting black holes, as a class, have longer recurrence times than similar systems containing less massive, accreting neutron stars (*14*).

Theoretically, it has been argued that the tidal perturbations caused by the companion star probably do not lead to much transport in the inner regions of the disks of close binaries because of their relatively large Mach numbers. This would be particularly true of the cold, quiescent disks considered here. However, no study to date has considered a realistic, steeply increasing profile of surface density with radius, as predicted for the quiescent disks by disk instability models (*9*). Because such a profile favors tidally induced transport in the inner regions of the disk (*23*), this question remains open.

The concept of accretion driven by MHD turbulence during outburst and by tidal perturbations during quiescence has several interesting implications. It complicates the modeling of the disks of transient close binaries because, in quiescence, α is plausibly nonuniform with radius, and it becomes time-variable as the disk shrinks and couples less and less with time to the tidal perturbation (a minimum value for the disk outer radius is set by the specific angular momentum of the accreted gas). It also allows for an efficiency of transport in quiescent disks that differs from system to system because it depends on the binary star parameters (*24*). Finally, it implies that, in the absence of a massive companion, weakly ionized disks must rely on yet another transport mechanism or they could be unable to accrete. Self-gravity is a plausible candidate for angular momentum transport in the disks of T-Tauri stars and active galactic nuclei, which are more massive than the disks considered here. However, in systems with disks similar to those of close binaries, such as supernova fallback disks or the disk that led to the planetary system around the pulsar PSR 1257+12, the absence of a massive companion could result in essentially passive disks.

References and Notes

1. J. Pringle, *Annu. Rev. Astron. Astrophys.* **19**, 137 (1981).
2. J. Frank, A. R. King, D. J. Raine, *Accretion Power in Astrophysics* (Cambridge Univ. Press, Cambridge, ed. 2, 1992).
3. N. I. Shakura and R. A. Sunyaev, *Astron. Astrophys.* **24**, 337 (1973).
4. S. A. Balbus and J. F. Hawley, *Astrophys. J.* **376**, 214 (1991).
5. _____, *Rev. Mod. Phys.* **70**, 1 (1998).
6. B. Warner, *Cataclysmic Variable Stars* (Cambridge Univ. Press, Cambridge, 1995).
7. F. Meyer and E. Meyer-Hofmeister, *Astron. Astrophys.* **104**, L10 (1981).
8. J. Smak, *Acta Astron.* **34**, 161 (1984).
9. J. K. Cannizzo, in *Accretion Disks in Compact Stellar Systems*, vol. 9 of *Advanced Series in Astrophysics and Cosmology*, J. C. Wheeler, Ed. (World Scientific, Singapore, 1993), pp. 6–40.
10. J. F. Hawley, C. F. Gammie, S. A. Balbus, *Astrophys. J.* **464**, 690 (1996).
11. T. P. Fleming, J. M. Stone, J. F. Hawley, *Astrophys. J.* **530**, 464 (2000).
12. C. F. Gammie and K. Menou, *Astrophys. J.* **492**, L75 (1998).
13. J.-M. Hameury, K. Menou, G. Dubus, J.-P. Lasota, J.-M. Huré, *Mon. Not. R. Astron. Soc.* **298**, 1048 (1998).
14. W. H. G. Lewin, J. van Paradijs, E. P. J. van den Heuvel, *X-ray Binaries* (Cambridge Univ. Press, Cambridge, 1995).
15. K. Menou, J.-M. Hameury, J.-P. Lasota, R. Narayan, *Mon. Not. R. Astron. Soc.* **314**, 498 (2000).
16. J. Papaloizou and J. E. Pringle, *Mon. Not. R. Astron. Soc.* **181**, 441 (1977).
17. P. Goldreich and S. Tremaine, *Astrophys. J.* **241**, 425 (1980).
18. M. Livio and H. Spruit, *Astron. Astrophys.* **252**, 189 (1991).
19. SU UMa–type dwarf novae show characteristic, long superoutbursts in addition to the more frequent normal outbursts of U Gem–type dwarf novae.
20. H. Ritter and U. Kolb, *Astron. Astrophys. Suppl.* **129**, 83 (1998) (via the Vizier online catalog).
21. A. R. King, *Q. J. R. Astron. Soc.* **29**, 1 (1988).
22. _____, U. Kolb, L. Burderi, *Astrophys. J.* **464**, L127 (1996).
23. G. J. Savonije, J. C. B. Papaloizou, D. N. C. Lin, *Mon. Not. R. Astron. Soc.* **268**, 13 (1994).
24. This could account for a value of α_{cold} in the quiescent disk of the low q dwarf nova WZ Sge, which is orders of magnitude less than what is usually inferred for other dwarf novae [J. Smak, *Acta Astron.* **43**, 101 (1993)].

25. I thank S. Balbus, C. Gammie, J. Goodman, B. Hansen, and R. Narayan for useful discussions. Supported by NASA through Chandra postdoctoral fellowship grant PF9-10006 awarded by the Chandra X-ray Center, which is operated by the Smithsonian Astrophysical Observatory for NASA under contract NAS8-39073.

14 March 2000; accepted 10 May 2000

Step-by-Step Engineered Multiparticle Entanglement

Arno Rauschenbeutel, Gilles Nogues, Stefano Osnaghi, Patrice Bertet, Michel Brune, Jean-Michel Raimond,* Serge Haroche

After quantum particles have interacted, they generally remain in an entangled state and are correlated at a distance by quantum-mechanical links that can be used to transmit and process information in nonclassical ways. This implies programmable sequences of operations to generate and analyze the entanglement of complex systems. We have demonstrated such a procedure for two atoms and a single-photon cavity mode, engineering and analyzing a three-particle entangled state by a succession of controlled steps that address the particles individually. This entangling procedure can, in principle, operate on larger numbers of particles, opening new perspectives for fundamental tests of quantum theory.

The quantum concepts of state superposition and entanglement can be used to process information in nonclassical ways (*1*). According to the superposition principle, a quantum system may exist at once in several eigenstates corresponding to different values of a physical observable (such as position, momentum, or spin). Entanglement is a consequence of this principle applied to composite systems. After quantum particles have interacted, their properties are not independent from each other. Instead, the composite system is described by a nonseparable entangled state, that is, a superposition of substates describing independent particles. Each of these substates corresponds to well-defined values of some set of observables (e.g., particles' positions). The system's state can also be expressed as a superposition of eigenstates for another set of noncommuting observables (e.g., particles' momenta). An entangled state can thus be put in different forms, each being adapted to the analysis of a specific detection procedure. An essential feature of entanglement is that a measurement performed on one part of the system determines the state of the other, whatever the distance between them.

Nonlocal two-particle correlations have been discussed by Einstein, Podolsky, and Rosen [the EPR situation (*2*)] and checked by many experiments, which have all vindicated quantum theory against classical interpretations (*3*). Beyond this fundamental aspect, manipulations of entangled states are essential for operations that process and transfer elements of information coded into quantum states (qubits) (*1*). State teleportation (*4–7*) and cryptographic key distribution (*8, 9*) have been performed with entangled photon beams. Recently, triplets of entangled photons have been generated and used for nonlocality tests (*10*).

Entanglement of massive particles instead of fast-escaping photons has also been considered, with the aim of building entangled states by reversible and controlled operations on individually addressed subsystems. Manipulations of spin particles have been dem-

Laboratoire Kastler Brossel, Département de Physique de l'Ecole Normale Supérieure, 24 rue Lhomond, 75231 Paris Cedex 05, France.

*To whom correspondence should be addressed. E-mail: jmr@lkb.ens.fr

onstrated with nuclear magnetic resonance (*11*). These experiments, however, involve macroscopic samples near thermal equilibrium without clear-cut entanglement (*12*). Reversible entanglement with massive particles has been realized only with trapped ions (*13, 14*) and with atoms and photons in a cavity (*15*). In ion experiments, an EPR pair (*13*) and, more recently, four-ion entanglement (*14*) have been generated. In those experiments, strong coupling requires the ions to be only a few micrometers apart, and the difficulty is to address them individually. The entangled multiparticle state is prepared in a collective process involving all qubits at once.

In contrast to ion traps, atom-cavity experiments manipulate particles at centimeter-scale distances, ideal conditions for separate qubit control (*16*). We report here an entanglement experiment involving three individually addressed Rydberg atoms, A_1, A_2, and A_3, and a field stored in a cavity mode C (*17*). Entanglement is produced by a sequence of one- and two-qubit operations, following a scheme proposed independently in (*18*) and (*19*). Two atoms (A_1 and A_2) and a zero- or one-photon field in C, all spatially separated, constitute the final entangled state. The third atom (A_3) is used to read out the cavity state. We have checked entanglement with measurements on two different sets of observables. This programmable entanglement process can, in principle, be generalized to more complex situations.

The experimental apparatus (Fig. 1) is similar to the one used in previous experiments (*15, 20–23*). The relevant atomic levels e, g, and i are circular Rydberg states with principal quantum numbers 51, 50, and 49, respectively (Fig. 1, upper inset). Rubidium atoms effusing from oven O are prepared in e or g inside box B (*24*). They cross a Gaussian cavity mode C (waist $w = 6$ mm), resonant on the 51.1-GHz $e \rightarrow g$ transition, before being counted by the field-ionization detector D. Classical pulses, produced by source S, can be applied on atoms before and after they interact with C, performing programmed transformations on each atomic state.

The cavity is made of superconducting niobium mirrors facing each other. A static electric field applied across the mirrors is used to control the atomic transition frequency through the Stark effect. An aluminum "ring," 50 mm in diameter, closing the aperture between the mirrors (shown open in Fig. 1 for the sake of clarity) reflects the photons scattered by surface imperfections back into C and increases their damping time to a value of 1 ms, longer than the duration of each experimental sequence. Inhomogeneous electric fields in the access holes to the ring destroy atomic coherences without affecting energy state populations. All coherent manipulations are thus performed inside the ring structure. At the beginning of each experimental sequence, C is prepared in the vacuum state $|0\rangle$ by a photon erasing procedure (*23*). The residual photon number, 0.1 after erasing, increases (as a result of thermal field leaks) to 0.3 at the end of the sequence.

The atomic velocity, $v = 503 \pm 2$ m/s, is fixed by a combination of pulsed Doppler-selective optical pumping and time-of-flight selection. With the laser excitation in B lasting 2 μs, the position of an atom is determined with a precision of ± 1 mm along its 20-cm path through the apparatus (enclosed in a 1.3 K cryostat), allowing each atom to be addressed independently. The Poissonian excitation process prepares 0.2, 0.4, and 0.2 circular atoms on average for A_1, A_2, and A_3, respectively. When D (detection efficiency $40 \pm 10\%$) registers one atom, the probability for a two-atom event is below 0.15, 0.25, and 0.15, respectively. Single-atom pulses are thus ensured at the expense of long averaging times (three-atom states created at a rate of 10 per second).

The joint atom-photon state manipulations rely on the resonant quantum Rabi rotation (*20*) experienced by each atom in C. The atom-cavity system undergoes oscillations between the states $|e,0\rangle$ and $|g,1\rangle$ (atom in e or g with either zero or one photon). The frequency of this oscillation at cavity center is $\Omega/2\pi = 47$ kHz. The full effective atom-cavity interaction time, $t_i = \sqrt{\pi} w/v$, corresponds to a 2π Rabi pulse. Shorter interaction times are obtained by using the Stark effect to switch the atomic transition away from cavity resonance at preset times.

By combining Rabi pulses of various durations on successive atoms, we progressively engineer an entangled state, one step at a time. Let us consider two important steps. If the system is initially in the $|e,0\rangle$ state, it evolves after a quarter of a period ($\pi/2$ Rabi pulse) into the atom-cavity EPR state

$$|\Psi_{EPR}\rangle = \frac{1}{\sqrt{2}} (|e,0\rangle + |g,1\rangle) \qquad (1)$$

(*15*). A second step involves a complete Rabi cycle (2π pulse). Starting from $|g,1\rangle$, the atom-cavity state undergoes a π phase shift: $|g,1\rangle \rightarrow -|g,1\rangle$. There is no such shift, however, if C is initially empty or if the atom is in the nonresonant state i. According to the superposition principle, an atom in g shifts the phase of a coherent photon state superposition by π: $|g\rangle(c_0|0\rangle + c_1|1\rangle) \rightarrow |g\rangle(c_0|0\rangle - c_1|1\rangle)$, where c_0 and c_1 are arbitrary probability amplitudes. In a complementary way, a single photon shifts the phase of an atomic coherence (amplitudes c_g and c_i) by π: $|1\rangle(c_g|g\rangle + c_i|i\rangle) \rightarrow |1\rangle(-c_g|g\rangle + c_i|i\rangle)$. These conditional phase shifts have been demonstrated in the operation of a quantum gate (*22*) and in an absorption-free detection of a single photon (*23*).

To demonstrate the engineered entanglement procedure, we chose to prepare a three-particle state analogous to the Greenberger, Horne, and Zeilinger (GHZ) spin triplet (*25*) according to a sequence of operations whose timing is sketched in Fig. 2A. We send across

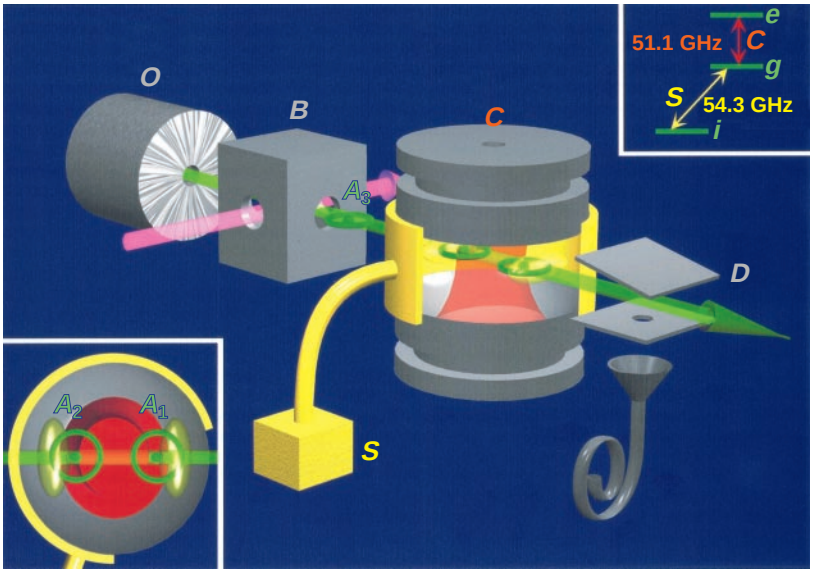

Fig. 1. The entangling machine. Rubidium atoms effusing from oven O are prepared in a circular state in zone B. Atomic orbits, shown in green, are not to scale. The upper inset presents the three relevant atomic energy levels. The atoms cross the superconducting cavity mode C (shown in red) and are detected at D. A ring around the cavity mirrors, shown open for clarity, increases the photon lifetime. A microwave source S prepares and analyzes quantum state superpositions. It couples to a standing wave structure inside the ring. Two antinode regions, where the atom is coupled to S, are shown in yellow. The lower inset presents a top view of the cavity (upper mirror removed).

C, initially empty, an atom A_1 initially in e. A $\pi/2$ Rabi pulse prepares the state described by Eq. 1. We then send atom A_2. Initially in g, it is prepared, before C, in the state $(|g\rangle + |i\rangle)/\sqrt{2}$ by a pulse P_2 produced by S. This atom interacts with C during its full cavity-crossing time (2π Rabi pulse). If A_1 left one photon in C, the A_2 coherence is phase-shifted by π. It stays unchanged if A_1 left C empty. The resulting A_1-A_2-C quantum state is

$$|\Psi_{\text{triplet}}\rangle = \tfrac{1}{2}[|e_1\rangle(|i_2\rangle + |g_2\rangle)|0\rangle + |g_1\rangle(|i_2\rangle - |g_2\rangle)|1\rangle] \quad (2)$$

where the state indices correspond to the atom numbers. Eq. 2 describes a three-particle entangled state and can be rewritten as

$$|\Psi_{\text{triplet}}\rangle = \tfrac{1}{2}[|i_2\rangle(|e_1,0\rangle + |g_1,1\rangle) + |g_2\rangle(|e_1,0\rangle - |g_1,1\rangle)] \quad (3)$$

describing an A_1-C EPR pair whose phase is conditioned to the A_2 state.

Because $|\Psi_{\text{triplet}}\rangle$ involves two levels for each subsystem, it is equivalent to an entangled state of three spins ½. Let us define the states $|+_i\rangle$ ($|-_i\rangle$) (with $i = 1, 2$) as $|+_1\rangle = |e_1\rangle$ ($|-_1\rangle = |g_1\rangle$), $|\pm_2\rangle = (|g_2\rangle \pm |i_2\rangle)/\sqrt{2}$, and $|+_C\rangle = |0\rangle$ ($|-_C\rangle = |1\rangle$). With these notations, $|\Psi_{\text{triplet}}\rangle$ takes the form of the GHZ three-spin state:

$$|\Psi_{\text{triplet}}\rangle = \frac{1}{\sqrt{2}}(|+_1,+_2,+_C\rangle - |-_1,-_2,-_C\rangle) \quad (4)$$

Other schemes have been proposed to realize multiparticle atom-cavity entanglement (*26, 27*).

We now discuss the detection of the $|\Psi_{\text{triplet}}\rangle$ state. We can detect atomic energy states but cannot directly detect the cavity field. However, the field can be copied onto a third atom A_3 that is detected afterward (*21*). The A_3-C interaction is set so that A_3, initially in g, is not affected if C is empty, but undergoes a π Rabi pulse in a single-photon field: $|g,0\rangle \rightarrow |g,0\rangle$ and $|g,1\rangle \rightarrow -|e,0\rangle$. Within a phase, A_3 maps the state of C. Thus, by detecting A_1, A_2, and A_3, we measure a set of observables belonging to the three parts of the entangled triplet. If A_3 crossed C before A_1 exited the ring, a three-atom entangled state $|\Psi'_{\text{triplet}}\rangle$ would be created between these two events:

$$|\Psi'_{\text{triplet}}\rangle = \tfrac{1}{2}[|e_1\rangle(|i_2\rangle + |g_2\rangle)|g_3\rangle - |g_1\rangle(|i_2\rangle - |g_2\rangle)|e_3\rangle] \quad (5)$$

$$= \tfrac{1}{2}[|i_2\rangle(|e_1,g_3\rangle - |g_1,e_3\rangle) + |g_2\rangle(|e_1,g_3\rangle + |g_1,e_3\rangle)] \quad (6)$$

Even if A_3 is delayed, its correlations with A_1 and A_2, which reflect those of C, are the same as those described in Eq. 6. In the following discussion, we thus refer equivalently to C or A_3.

Checking the A_1-A_2-C entanglement involves measurements in two different bases. A microwave pulse after the interaction with C, followed by energy detection in D, allows us to probe each atom's pseudo-spin along an arbitrary "quantization axis." In experiment I (Fig. 2B), we checked "longitudinal" correlations by detecting the "spins" along what we define as the "z axis" (eigenstates $|\pm_i\rangle$ for $i = \{1,2\}$ and $|+_3\rangle = |e_3\rangle$ and $|-_3\rangle = |g_3\rangle$ for A_3). For A_1 and C (i.e., A_3), this is a direct energy detection. For A_2, a $\pi/2$ analysis pulse $R_2^{(I)}$ on the $i \rightarrow g$ transition transforms $|+_2\rangle$ and $|-_2\rangle$ into, respectively, $|i_2\rangle$ and $|g_2\rangle$. The three atoms should thus be detected in $\{e_1,i_2,g_3\}$ or $\{g_1,g_2,e_3\}$ with equal probabilities. However, these correlations, taken alone, can be explained classically (statistical mixture of $|e_1,i_2,g_3\rangle$ and $|g_1,g_2,e_3\rangle$ states).

A second experiment is required to test the quantum nature of the superposition. In experiment II (Fig. 2C), we studied "transverse correlations" by detecting A_1 and A_2 along the "x axis" [eigenstates $|\pm_{x,i}\rangle = (|+_i\rangle \pm |-_i\rangle)/\sqrt{2}$]. A_3 is detected along an axis in the horizontal plane at an angle ϕ from the x direction [eigenstates $|\pm_{\phi,3}\rangle = (|+_3\rangle \pm \exp(+i\phi)|-_3\rangle)/\sqrt{2}$]. Atom A_2 is directly detected in D, because $|\pm_{x,2}\rangle$ coincide with $|g_2\rangle$ and $|i_2\rangle$. A_1 and A_3 undergo, after C, two analysis $\pi/2$ pulses $R_1^{(II)}$ and $R_3^{(II)}$ on the $e \rightarrow g$ transition, with a phase difference ϕ. A detection in g amounts to a detection in $|+_x\rangle$ or $|+_\phi\rangle$ for A_1 and A_3, respectively, at the exit of C.

For the sake of clarity, let us first consider the case of only two atoms (1 and 3) in state $|\Psi'_{\text{EPR}}\rangle$:

$$|\Psi'_{\text{EPR}}\rangle = \frac{1}{\sqrt{2}}(|e_1,g_3\rangle - |g_1,e_3\rangle) \quad (7)$$

These atoms are analyzed along the x and ϕ directions, respectively. When A_1 is detected in $|+_{x,1}\rangle$ (i.e., g_1 in D), A_3 is projected onto $|-_{x,3}\rangle$, because $|\Psi'_{\text{EPR}}\rangle$ is the rotation-invariant spin singlet. Hence, the detection probability of A_3 in $|+_{\phi,3}\rangle$ (i.e., g_3 in D) oscillates between 1 (for $\phi = \pm\pi$) and 0 (for $\phi = 0, 2\pi$): "Fringes" observed in the joint detection probabilities of the two atoms (*15*) show that quantum coherence has been transferred between them through the EPR correlations. The phase of the fringes would be shifted by π if the minus sign in Eq. 7 were changed into a plus. Returning to the three-system case, Eq. 6 shows that similar fringes are expected for the joint detection of A_1 and A_3 corresponding to a given state for A_2. They have the same phase as the EPR fringes described by Eq. 7 when A_2 is in i_2. They are shifted by π when A_2 is in g_2. This shift results from the action of the A_2-C phase gate (*22*) on the A_1-C EPR pair.

A tight timing is required to have A_1 and A_2 simultaneously inside the ring. A_2 interacts with C for the full atom-cavity interaction time. The π Rabi pulse condition for A_3 is realized with the Stark switching technique. Atom A_1 couples to C 75 μs after the erasing sequence, and should undergo a $\pi/2$ Rabi rotation. It is followed by A_2 after a delay of 25 μs. The separation between A_1 and A_2 is 1.2 cm, twice the

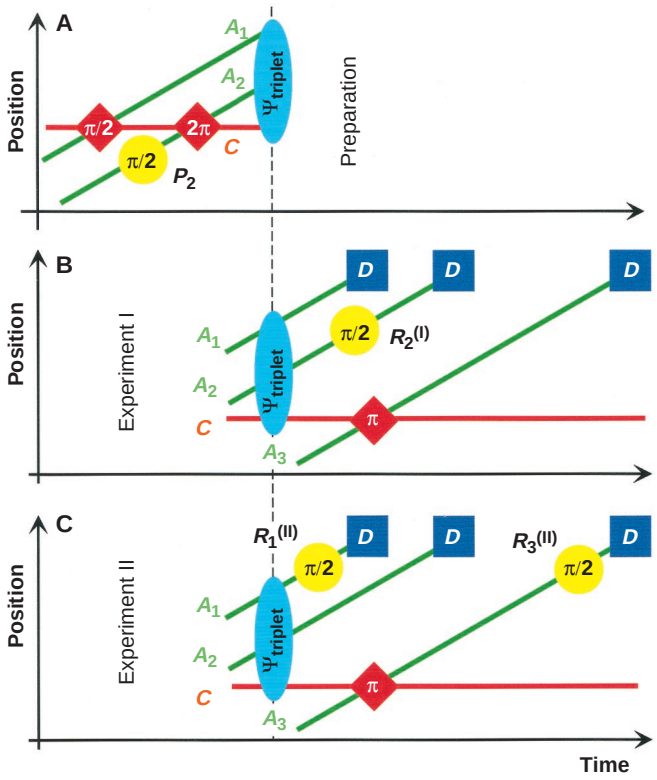

Fig. 2. The entanglement procedure. The atoms and cavity space lines during the experiments are represented qualitatively. Red diamonds, atom-cavity interactions; yellow circles, classical pulses produced by S; dark blue squares, detection events. (**A**) Preparation of the entangled state $|\Psi_{\text{triplet}}\rangle$. (**B**) Experiment I: detection of "longitudinal" correlations. (**C**) Experiment II: detection of "transverse" correlations.

cavity waist. Nevertheless, A_1 still interacts with C when A_2 starts its 2π Rabi rotation. Because both atoms experience the same shift, a simple Stark-tuning scheme is not adequate for A_1. This atom is left resonant with C until the state $|\Psi_{EPR}\rangle$ (Eq. 1) is prepared, before A_2 couples to C. In classical terms, the field is in quadrature with the atomic dipole. A short (τ = 2 μs) dc electric field pulse is then applied, shifting the atomic transition frequency out of resonance by $\Delta/2\pi = 1/4\tau$. At the end of this pulse, the resonance is restored, before A_2 couples to C. However, the phase of the A_1 dipole has been shifted by $\Delta\tau = \pi/2$. The dipole and the cavity field are now in phase and, within unimportant phase changes, A_1 does not interact any longer with C. With this timing, we prepare an entangled A_1-A_2-C triplet inside the ring structure. A numerical simulation of the A_1-A_2-C evolution shows that $|\Psi_{triplet}\rangle$ is prepared with a 96% probability. Atom A_1, however, has exited the ring before A_3 has crossed C, following A_2 after a delay of 75 μs. This timing thus prevents the preparation of $|\Psi'_{triplet}\rangle$ (Eq. 5). As discussed above, the A_1-A_2-A_3 correlations nonetheless demonstrate the A_1-A_2-C entanglement.

The pulses P_2, $R_2^{(I)}$, $R_1^{(II)}$, and $R_3^{(II)}$ produced by S create a low–quality factor standing wave inside the ring, whose map has been determined independently. We apply the pulses when the atom is in an antinode of this wave. Selective pulses may be applied on A_1 and A_2 even if both are simultaneously in the ring, one in a node, the other in an antinode. In experiment I, P_2 and $R_2^{(I)}$ are applied on A_2 on the 54.3-GHz $g \rightarrow i$ transition. These pulses, off-resonant with C, do not couple to it. In experiment II, $R_1^{(II)}$ and $R_3^{(II)}$ are used to probe the $|\pm_{x,1}\rangle$ and $|\pm_{\phi,3}\rangle$ states. A pulse resonant on the $e \rightarrow g$ transition would couple in C through scattering on the mirror's imperfections. A field would then build up in C and spoil quantum correlations. To avoid this, we first apply a π pulse on the $g \rightarrow i$ transition, transforming the e-g coherence into an e-i one. A $\pi/2$ pulse on the two-photon $e \rightarrow i$ transition at 52.7 GHz, which does not feed any field in C, is then used to probe this coherence. States $|+_{x,1}\rangle$ ($|-_{x,1}\rangle$) and $|+_{\phi,3}\rangle$ ($|-_{\phi,3}\rangle$) are mapped by this effective three-photon $\pi/2$ pulse onto i_1 (e_1) and i_3 (e_3), respectively.

The results of experiment I (Fig. 3) are presented as histograms giving the probabilities for detecting the atoms in the eight relevant channels (*28*). As expected, the $\{e_1,i_2,g_3\}$ and $\{g_1,g_2,e_3\}$ channels dominate. The total probability of these channels is $P_{\parallel} = 0.58 \pm 0.02$. The difference between them is due to experimental imperfections. Because channel $\{g_1,g_2,e_3\}$ corresponds to one photon stored in the cavity between A_1 and A_3, it is sensitive to field relaxation and leaks into the other $\{g_1\}$ channels. Events with two atoms in the same sample, residual thermal fields, and detection errors also contribute to the population of the parasitic channels.

For the signals of experiment II (Fig. 4), the relative phase ϕ of $R_3^{(II)}$ and $R_1^{(II)}$ is adjusted by tuning the frequency of the source inducing the $e \rightarrow i$ two-photon transition. Figure 4A presents the probability $P(+_{\phi,3};+_{x,1})$ for detecting A_3 in i (i.e., $|+_{\phi,3}\rangle$) provided A_1 has also been detected in i (i.e., $|+_{x,1}\rangle$). The green circles give this conditional probability when A_2 is not sent. The observed fringes correspond to the two-atom EPR pair situation. The blue circles give the corresponding conditional probability when A_2 is detected in i. Because of very long acquisition times (8 hours for the data in Fig. 4), signals have been recorded only for three phase values. The red squares correspond to a detection of A_2 in g. The A_1-A_3 correlations are not modified when A_2 is detected in i. When A_2 is detected in g, the A_1-A_3 EPR fringes are shifted by π, as expected. All joint probabilities corresponding to the four possible outcomes for A_1 and A_3 are combined to produce the "Bell signal" (*3*), which is the expectation value $\langle\sigma_{x,1}\sigma_{\phi,3}\rangle = P_{i1,i3} + P_{e1,e3} - P_{i1,e3} - P_{e1,i3}$, where the σ's are Pauli matrices associated to the pseudo-spins and $P_{a1,b3}$ is the probability for detecting A_1 in a and A_3 in b ($\{a,b\} = \{i,e\}$). In a plot of the Bell signal versus ϕ (Fig. 4B, with the same color codes as in Fig. 4A), the π phase shift of the A_1-A_3 EPR correlations, conditioned to the A_2 state, is conspicuous. The fringes' amplitude (or visibility) is $2V_{\perp} = 0.28 \pm 0.04$.

Because of experimental imperfections, the first stage of our experiment (Fig. 2A) does not prepare the pure state $|\Psi_{triplet}\rangle$, but rather a

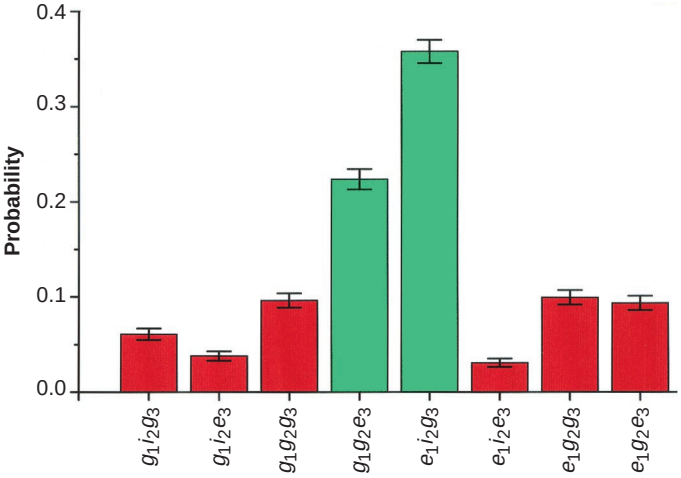

Fig. 3. Longitudinal correlations (experiment I). Histograms of the detection probabilities for the eight relevant detection channels are shown. The two expected channels g_1,g_2,e_3 and e_1,i_2,g_3 clearly dominate the others, which are populated by spurious processes. The error bars correspond to the binomial statistics variance.

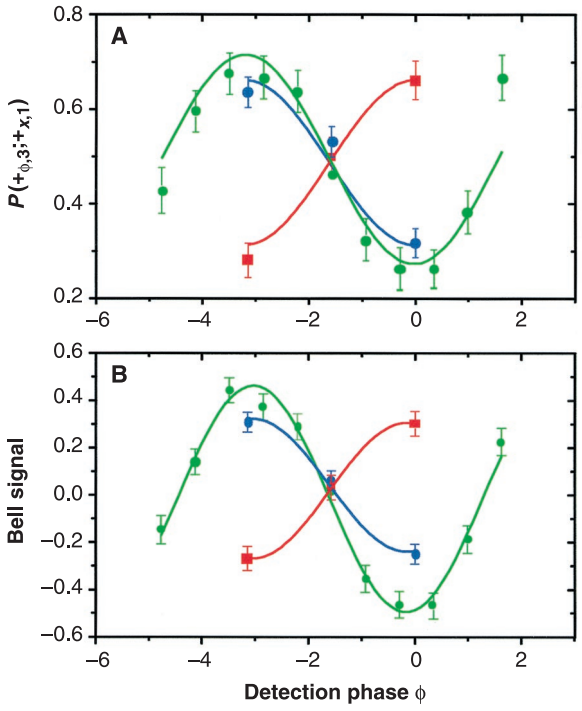

Fig. 4. Transverse correlations (experiment II). (**A**) Probability $P(+_{\phi,3};+_{x,1})$, versus the detection phase ϕ, for detecting A_3 in i if A_1 has also been detected in i. Green circles, no A_2 atom; blue circles, atom A_2 detected in i; red squares, atom A_2 detected in g. (**B**) Bell signal versus ϕ with the same color code as in (A). In both (A) and (B), the π phase shift of the A_1-A_3 EPR correlations conditioned to the state of A_2 is observed. Error bars are as in Fig. 3. Solid lines are sine fits.

mixed state described by a density matrix ρ. The setup efficiency is thus characterized by a fidelity $F = \langle \Psi_{triplet} | \rho | \Psi_{triplet} \rangle$. If the detection stages (Fig. 2, B and C) were perfect, F would be equal to the sum $P_{\parallel}/2 + V_{\perp}$ (*14*). However, the value of this quantity, 0.43, is affected by known detection errors and F is actually larger. Trivial imperfections can occur at three different stages: the mapping of the cavity state onto A_3; the classical microwave pulses $R_2^{(I)}$, $R_1^{(II)}$, and $R_3^{(II)}$; and the energy state–selective atom counting. We have determined these errors independently by additional single-atom experiments. Taking them into account, we determine a fidelity $F = 0.54 \pm 0.03$. The three kinds of errors listed above account respectively for corrections of 0.03, 0.05, and 0.03 to the raw 0.43 value. The fact that F is larger than 0.5 ensures that genuine three-particle entanglement is prepared here (*14*).

The combined results of experiments I and II demonstrate the step-by-step engineered entanglement of three qubits, manipulated and addressed individually. By adjusting the various pulses, the experiment could be programmed to prepare a tailored three-particle state. One drawback of our apparatus is that atomic coherences cannot exit the cavity-ring structure. There are now good prospects for realizing a better cavity without any ring, relaxing the tight timing constraints and improving the fidelity. At present, the main limitation is that circular atoms are prepared with Poisson statistics with a low mean value, requiring long data acquisition times. However, it is possible to implement preparation techniques for circular states that generate exactly one atom on demand. For instance, the fluorescence from a weak atomic beam can be used to image a single atom and excite it deterministically to the circular state in a fully adiabatic process. With these improvements, the techniques described here could be extended to more complex systems.

Tests of quantum nonlocality on many-particle generalizations of the GHZ triplet (*29*) are particularly appealing. These states are generated by a simple iteration of the present scheme (*18, 19*). After having prepared the A_1-C pair in the state described by Eq. 1, one sends a stream of atoms A_2-A_3- . . . A_n all prepared in $(|i\rangle + |g\rangle)/\sqrt{2}$ and undergoing, if in g, a 2π Rabi rotation in a single-photon field. Because this rotation does not change the photon number, the zero- and one-photon parts of the A_1-C system become correlated to an A_2-A_3- . . . A_n state, with all $n - 1$ atoms in $(|i\rangle + |g\rangle)/\sqrt{2}$ for the zero-photon and in $(|i\rangle - |g\rangle)/\sqrt{2}$ for the one-photon part, preparing the entangled state

$$|\Psi\rangle = \frac{1}{\sqrt{2}} (|+_1, +_2, \ldots, +_C\rangle - |-_1, -_2, \ldots, -_C\rangle) \quad (8)$$

Teleportation experiments operating on massive particles instead of photons are also within reach with an improved version of the setup (*30*).

References and Notes

1. C. H. Bennett and D. P. DiVincenzo, *Nature* **404**, 247 (2000).
2. A. Einstein, B. Podolsky, N. Rosen, *Phys. Rev.* **47**, 777 (1935).
3. A. Zeilinger, *Rev. Mod. Phys.* **71**, S288 (1998).
4. C. H. Bennett *et al.*, *Phys. Rev. Lett.* **70**, 1895 (1993).
5. J.-W. Pan *et al.*, *Nature* **390**, 575 (1998).
6. D. Boschi, S. Branca, F. De Martini, L. Hardy, S. Popescu, *Phys. Rev. Lett.* **80**, 1121 (1998).
7. A. Furusawa *et al.*, *Science* **282**, 706 (1998).
8. C. H. Bennett, G. Brassard, A. Ekert, *Sci. Am.* (October 1992), p. 50.
9. J. G. Rarity, P. C. M. Owens, P. R. Tapster, *J. Mod. Opt.* **41**, 2435 (1994).
10. J. W. Pan, D. Bouwmeester, M. Daniell, H. Weinfurter, A. Zeilinger, *Nature* **403**, 515 (2000).
11. N. A. Gershenfeld and I. L. Chuang, *Science* **275**, 350 (1997).
12. S. L. Braunstein *et al.*, *Phys. Rev. Lett.* **83**, 1054 (1999).
13. Q. A. Turchette *et al.*, *Phys. Rev. Lett.* **81**, 3631 (1998).
14. C. A. Sackett *et al.*, *Nature* **404**, 256 (2000).
15. E. Hagley *et al.*, *Phys. Rev. Lett.* **79**, 1 (1997).
16. P. Domokos, J. M. Raimond, M. Brune, S. Haroche, *Phys. Rev. A* **52**, 3554 (1995).
17. A three–atom-cavity experiment was recently reported [B. T. H. Varcoe, S. Brattke, M. Weidinger, H. Walther, *Nature* **403**, 743 (2000)]. It exhibited atomic energy correlations but did not detect entanglement.
18. S. Haroche *et al.*, in *Laser Spectroscopy 14,* R. Blatt, J. Eschner, D. Leibfried, F. Schmidt-Kaler, Eds. (World Scientific, New York, 1999), pp. 140–149.
19. S. B. Zheng, *J. Opt. B* **1**, 534 (1999).
20. M. Brune *et al.*, *Phys. Rev. Lett.* **76**, 1800 (1996).
21. X. Maître *et al.*, *Phys. Rev. Lett.* **79**, 769 (1997).
22. A. Rauschenbeutel *et al.*, *Phys. Rev. Lett.* **83**, 5166 (1999).
23. G. Nogues *et al.*, *Nature* **400**, 239 (1999).
24. P. Nussenzveig *et al.*, *Phys. Rev. A* **48**, 3991 (1993).
25. D. M. Greenberger, M. A. Horne, A. Zeilinger, *Am. J. Phys.* **58**, 1131 (1990).
26. S. Haroche, *Ann. N.Y. Acad. Sci.* **755**, 73 (1995).
27. B. T. H. Varcoe, S. Brattke, B.-G. Englert, H. Walther, in *Laser Spectroscopy 14,* R. Blatt, J. Eschner, D. Leibfried, F. Schmidt-Kaler, Eds. (World Scientific, New York, 1999), pp. 130–139.
28. Because the experiment involves three levels for each atom, there are 27 detection channels in all. We only give the channels corresponding to the relevant transitions for each atom: $e \rightarrow g$ for A_1 and A_3; $g \rightarrow i$ for A_2. The other channels are weakly populated by spurious effects such as spontaneous emission outside C, residual thermal photons, influence of the $R_2^{(I)}$ or P_2 pulses on the other atoms, and absorption of the cavity field by A_2 as a result of imperfect 2π Rabi rotation. The total contribution of these transfer processes is less than 15%.
29. N. D. Mermin, *Phys. Rev. Lett.* **65**, 1838 (1990).
30. L. Davidovich, N. Zagury, M. Brune, J. M. Raimond, S. Haroche, *Phys. Rev. A* **50**, R895 (1994).

31. Laboratoire Kastler Brossel is a Unité Mixte de Recherche, Ecole Normale Supérieure, Université Pierre et Marie Curie et CNRS (UMR8552). Supported in part by the European Community and Japan Science and Technology Corporation (International Cooperative Research Project, Quantum Entanglement project). We thank P. Goy and M. Gross for help with the microwave technology.

29 March 2000; accepted 20 April 2000

Assessment of Oceanic Productivity with the Triple-Isotope Composition of Dissolved Oxygen

Boaz Luz* and Eugeni Barkan

Plant production in the sea is a primary mechanism of global oxygen formation and carbon fixation. For this reason, and also because the ocean is a major sink for fossil fuel carbon dioxide, much attention has been given to estimating marine primary production. Here, we describe an approach for estimating production of photosynthetic oxygen, based on the isotopic composition of dissolved oxygen of seawater. This method allows the estimation of integrated oceanic productivity on a time scale of weeks.

Our knowledge of the rate of marine photosynthetic production is based primarily on bottle incubation experiments (*1*). These experiments provide local instantaneous primary production rates, which often miss the effects of significant blooms because of the heterogeneous distribution of plankton in time and space. A broader view of marine primary production can be obtained from satellite remote sensing (*2*). However, values derived by this method depend on the quality of calibration data obtained by actual productivity measurements in the ocean and cannot be better than the accuracy of this information. Here, we present a way to estimate marine production that alleviates the inherent problems of incubation methods. In this approach, gross production, integrated on spatial and temporal scales, is estimated from the difference between the triple isotope (^{16}O, ^{17}O, and ^{18}O) composition of atmospheric and dissolved O_2 and the rate of air-sea O_2 exchange.

Most terrestrial processes fractionate O isotopes in a mass-dependent way, such that ^{17}O

The Institute of Earth Sciences, The Hebrew University of Jerusalem, Jerusalem 91904, Israel.

*To whom correspondence should be addressed.

Step-by-Step Engineered Multiparticle Entanglement

Arno Rauschenbeutel *et al.*

Science **288**, 2024 (2000);
DOI: 10.1126/science.288.5473.2024